

## Article

# Fast Identification of Micro-Health Parameters for Retired Batteries Based on a Simplified P2D Model by Using Padé Approximation

Jianing Xu<sup>1,\*</sup>, Chuanyu Sun<sup>1,\*</sup> , Yulong Ni<sup>1</sup>, Chao Lyu<sup>1,\*</sup> , Chao Wu<sup>2</sup>, He Zhang<sup>1</sup>, Qingjun Yang<sup>3</sup> and Fei Feng<sup>4,\*</sup>

<sup>1</sup> School of Electrical Engineering and Automation, Harbin Institute of Technology, Harbin 150001, China

<sup>2</sup> Department of Electrical Engineering and Automation, Luoyang Institute of Science and Technology, Luoyang 471023, China

<sup>3</sup> School of Mechatronics Engineering, Harbin Institute of Technology, Harbin 150001, China

<sup>4</sup> School of Automation, Chongqing University, Chongqing 400044, China

\* Correspondence: chuanyu.sun@mail.polimi.it (C.S.); lu\_chao@hit.edu.cn (C.L.); feifeng@cqu.edu.cn (F.F.)

**Abstract:** Better performance consistency of regrouped batteries retired from electric vehicles can guarantee the residual value maximized, which greatly improves the second-use application economy of retired batteries. This paper develops a fast identification approach for micro-health parameters characterizing negative electrode material and electrolyte in LiFePO<sub>4</sub> batteries on the basis of a simplified pseudo two-dimensional model by using Padé approximation is developed. First, as the basis for accurately identifying micro-health parameters, the liquid-phase and solid-phase diffusion processes of pseudo two-dimensional model are simplified based on Padé approximation, especially according to enhanced boundary conditions of liquid-phase diffusion. Second, the reduced pseudo two-dimensional model with the lumped parameter is proposed, the target parameters characterizing negative electrode material ( $\epsilon_n$ ,  $D_{s,n}$ ) and electrolyte ( $D_e$ ,  $C_e$ ) are grouped with other unknown but fixed parameters, which ensures that no matter whether the target parameters can be achieved, the corresponding varying traces is able to be effectively and independently monitored by lumped parameters. Third, the fast identification method for target micro-health parameters is developed based on the sensitivity of target parameters to constant-current charging voltage, which shortens the parameter identification time in comparison to that obtained by other approaches. Finally, the identification accuracy of the lumped micro-health parameters is verified under 1 C constant-current charging condition.

**Keywords:** LiFePO<sub>4</sub> battery; micro-health parameter; reduced P2D model; parameter identification; Padé approximation; second-use application



**Citation:** Xu, J.; Sun, C.; Ni, Y.; Lyu, C.; Wu, C.; Zhang, H.; Yang, Q.; Feng, F. Fast Identification of Micro-Health Parameters for Retired Batteries Based on a Simplified P2D Model by Using Padé Approximation. *Batteries* **2023**, *9*, 64. <https://doi.org/10.3390/batteries9010064>

Academic Editor: Carlos Ziebert

Received: 28 November 2022

Revised: 8 January 2023

Accepted: 13 January 2023

Published: 16 January 2023



**Copyright:** © 2023 by the authors. Licensee MDPI, Basel, Switzerland. This article is an open access article distributed under the terms and conditions of the Creative Commons Attribution (CC BY) license (<https://creativecommons.org/licenses/by/4.0/>).

## 1. Introduction

Electric vehicles (EVs) have become more and more popular in recent years, which can effectively face the global energy crisis [1]. Lithium-ion batteries have been widely used for EV applications, given their long cycle life, high energy density, and environmental friendliness [2,3]. When the performance of the on-board batteries cannot meet the EV mileage and safety standards, many retired batteries need to be treated urgently [4]. Second-use application is the optimal solution for retired EV batteries to effectively avoid energy waste and use the remaining value of retired batteries [5]. However, the long-time performance tests increase the second-use application cost, and the regular classification basis (battery capacity or internal resistance) cannot guarantee the consistency of regrouped retired batteries, which will accelerate the battery performance degradation [6,7]. To enhance the rapid growth of the second-use application of retired batteries from EVs, the fast performance test strategy and multi-dimensional classification basis supply need to be well proposed. Fast providing the multi-dimensional classification basis for retired batteries can

effectively improve the performance consistency of regrouped batteries, which promotes to release of the maximum available capacity and increases the economic value for second-use application.

In our previous study, we have proposed the fast capacity estimation method and the fast accelerated degradation fault diagnose under the larger rate constant-current charging condition [6], and this study will focus on the identification of the micro-health parameters method under the same charging condition, which can improve the test efficiency and add the classification basis for retired batteries. The micro-health parameters stand for the performance of active material and electrolyte inside the battery, and the changes in the micro-health parameters can present the battery internal health state.

The complicated physico-chemical features of the battery have been depicted by a number of partial differential equations of the pseudo-two-dimensional (P2D) model, which has been frequently employed in research on lithium-ion battery performance [8]. The influencing parameters in the P2D model intuitively reflects the performance of electrolyte and internal active material. The particular characteristics of the P2D model are the micro-health parameters to be determined, which will offer the multi-dimensional classification foundation for retired batteries [9]. To effectively identify the micro-health parameters to analyze the internal health state by the P2D model, two problems need to be solved: (1) the simplification method of the complex P2D model; (2) the unambiguous identification method of the micro-health parameters.

For the first problem, since the P2D model is composed of multiple partial differential equations and the complicated calculation limits the practical application possibility, lots of researchers have carried out the P2D model simplification technology. Guo et al., first proposed the single-particle (SP) model of lithium-ion batteries. The SP model equates the porous structure of the electrode materials to a single particle and omits the calculation of the liquid-phase diffusion process, which greatly reduces computational complexity [10,11]. Since the SP model accuracy is low under the larger current charging or discharging condition, some researchers have subsequently added the control equations describing the liquid-phase diffusion process based on the SP model [12,13]. In addition, some other researchers have considered the problem of uneven current density distribution and developed the extended single-particle (ESP) model [14,15]. When the battery model structure is determined, the partial differential equations of the P2D model describing the electrochemical processes need to be simplified to realize the practical application. Among lots of studies, R.E. White and V.R. Subramanian have made outstanding contributions. In 2001, they first proposed the method of solving partial differential equations with boundary conditions in the P2D model. To further improve the calculation speed, they successively applied the separation variable [16], polynomial fitting [17], and orthogonal decomposition methods [18,19] to the control equation simplification of P2D model. Since the simplified model accuracy based on the above approximation methods is relatively low, the Páde approximation, fractional-order approximation, and Galerkin approximation methods have also been applied to the P2D model, which shows better accuracy simulating the battery charging and discharging behaviors [20–22].

For the second problem, to effectively extract the battery micro-health parameters at different aging stages, researchers have carried out relevant studies on the specific parameter identification of the P2D model and analyzed the changing laws of different micro-health parameters during the aging process to study performance changes in active materials and electrolyte inside the battery. R.E. White research group also carried out related work earlier. They used the Levenberg-Marquardt algorithm to achieve the identification of solid-phase diffusion coefficients under 1/5 C, 1/2 C, 1 C, and 2 C constant-current discharging conditions [23,24]. A. Jokar et al., employed the genetic algorithm to recognize eight micro-health parameters including the initial lithium insertion of electrode and diffusion coefficients, etc., under 1/10 C, 1 C, 2 C, and 5 C constant-current discharging conditions [25,26]. After that, they tried to use the neural network method to realize the parameter identification including the solid-phase diffusion coefficient and electrochemical reac-

tion coefficient [27]. In addition, X. Han et al., identified the active material volume fraction related to battery capacity to analyze battery capacity degradation performance [28]. R. Masoudi et al., used the homotopy optimization method to identify the number of lithium ions in the electrolyte, the solid-phase conductivity of the negative electrode, and the initial electrolyte concentration under the constant-current charging condition [29]. Since the above methods depend on lots of known parameters, L. Zhang et al., designed dynamic working conditions for parameter identification of LiFePO<sub>4</sub>/graphite and LiCoO<sub>2</sub>/graphite batteries and identified more than 20 parameters of P2D model [30,31]. J. Li et al., first use the 1/50 C constant-current discharge condition to identify the initial lithium insertion rate of the positive and negative electrodes and parameters that vary with the battery aging, then the battery internal resistance is calibrated using the battery impedance test equipment. Finally, the parameters characterizing the electrochemical reaction polarization and electrolyte concentration polarization are achieved under the dynamic pulse condition [31]. X. Li et al., investigated the effect of the change for characteristic parameters of the P2D model on the battery terminal voltage under constant-current charging condition. The parameters characterizing the solid-phase diffusion ability of positive and negative electrode under the high and low charging SOC interval, respectively. Parameters bound up with the ohmic resistance, and the liquid-phase diffusion ability are identified under the dynamic discharge conditions [32].

Although the above model simplification methods and parameter identification methods can extract the micro-health parameters in the P2D model, these methods cannot be employed directly to the retired batteries with the two remarkable issues: (1) the coupling effects of non-target parameters on target parameters are difficult to be eliminated based on the above simplified models, (2) the designed multi-step test conditions for parameter identification increase the test cost of second-use application. In this study, the identification method of micro-health parameters characterizing the negative electrode active material and electrolyte performance for retired LiFePO<sub>4</sub> batteries is proposed with two significant contributions. On one hand, the simplified P2D model with lumped parameters based on Padé approximation is developed. In the simplified model, the parameters characterizing negative electrode active material and electrolyte performance are linked to other parameters that are constant, not only reducing the quantity of parameters to be identified but also dispelling the coupling effects between various target parameters and other parameters. Hence, even the particular values of target parameters are not able to be directly obtained, their varying traces may still be observed effectively based on the lumped parameters. On the other hand, based on the sensitivity analysis results of target parameters on the charging voltage, the identification strategy for the micro-health parameters characterizing negative electrode active material and electrolyte performance under the larger rate constant-current charging condition is proposed. Combined with our previous work, the target micro-health parameters and battery capacity can be achieved under the same test condition, which can fast provide the multi-dimensional classification basis for retired batteries.

In line with these objectives, this study is organized as follows. In Section 2, the simplified P2D model with lumped parameters based on Padé approximation is developed. In Section 3, the identification strategy for the micro-health parameters characterizing negative electrode active material and electrolyte performance is proposed. In Section 4, the identification results of micro-health parameters are discussed and analyzed, compared with the other two methods. Finally, conclusions are summarized in Section 5.

## 2. The Reduced P2D Model Establishment with Lumped Micro-Health Parameters

In the P2D model, the active material particles of positive electrode and negative electrode are equivalent to spherical particles. This study assumes that all the reactions inside the electrode are distributed uniformly over all the particles. The direction from the positive/negative electrode to the negative/positive electrode through the electrolyte is defined as the  $x$  direction, and the transport direction of lithium-ions in the active particle is de-

defined as the  $r$  direction, which is the radius direction of the active particle. Figure 1 shows the P2D model schematic diagram, where  $L_n$  is the thickness of negative electrode region;  $L_p$  is the thickness of positive electrode region;  $L_s$  is the thickness of separator region.

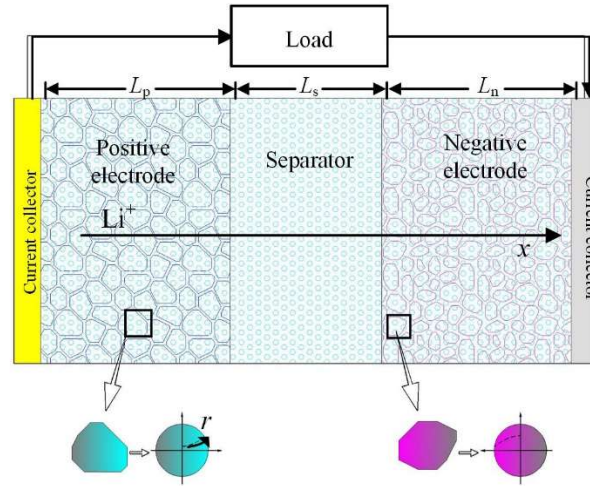


Figure 1. The schematic diagram of P2D model.

Although the physical meaning of micro-health parameters in the P2D model is clear, the mutual coupling between model parameters makes the identification of target parameters challenging. In this section, Padé approximation and parameter-lumped methods are employed to simplify the P2D model, ensuring that even through the particular values of target micro-health parameters may not be achieved, their varying traces may still be observed independently and effectively by the corresponding lumped parameters, and the undesired coupling effects between target parameters and other non-targeted parameters can also be eliminated.

### 2.1. Approximation of Solid-Phase Diffusion Process of P2D

In the P2D model, the solid-phase diffusion process of lithium-ions inside battery active particles can be described by Equation (1). The left side of Equation (1) stands for the variation in dynamic solid-phase concentration over time, while the right side represents the diffusion process of lithium-ion inside active particles based on Fick’s second law.

During the charging and discharging process of lithium-ion batteries, the solid-phase concentration gradient is generated inside the active particles of the electrode material. The concentration gradient at the center of the particle is zero, and the concentration gradient at the particle surface is determined by the lithium-ion solid-phase diffusion coefficient and the flow rate of the pore wall, thus, the boundary condition of the solid-phase diffusion process of the P2D model is given by Equation (2).

$$\frac{\partial C_{s,k}(r, t)}{\partial t} = D_{s,k} \frac{1}{r^2} \frac{\partial}{\partial r} \left( r^2 \frac{\partial C_{s,k}(r, t)}{\partial r} \right) \quad k = p, n \quad (1)$$

$$\begin{cases} \frac{\partial C_{s,k}}{\partial t} \Big|_{r=0} = 0 \\ \frac{\partial C_{s,k}}{\partial t} \Big|_{r=R_{s,k}} = -\frac{J_k(t)}{D_{s,k}} \end{cases} \quad k = p, n \quad (2)$$

where  $C_{s,k}$  is the solid-phase concentration of lithium-ion that changes with the charging or discharging time,  $D_{s,k}$  is the solid-phase diffusion coefficient of lithium ions,  $J_k$  is pore wall flow rate,  $r$  is active particle radius,  $r = 0$  represents the active particle center,  $r = R_s$  represents the active particle surface,  $R_s$  represents the particle radius,  $p$  stands for the positive electrode,  $n$  indicates the negative electrode, and  $t$  is the charging or discharging time.

Taking the Laplace transform to the variable  $t$  of Equation (1), the general solution for  $C_{s,k}$  in Equation (1) is solved as:

$$C_{s,k}(r, s) = \frac{D_1}{r} \exp\left(r\sqrt{\frac{s}{D_{s,k}}}\right) + \frac{D_2}{r} \exp\left(-r\sqrt{\frac{s}{D_{s,k}}}\right) \tag{3}$$

where  $D_1$  and  $D_2$  are the coefficients that should be determined.

Substituting boundary conditions Equation (2) into Equation (3), the standard transfer function expression of  $C_{s,k}$  can be obtained as:

$$\frac{C_{s,k}(s)}{J_k(s)} = \frac{R_{s,k}^2}{D_{s,k}r} \frac{\sinh(r\sqrt{s/D_{s,k}})}{\sinh(r\sqrt{s/D_{s,k}}) - R_{s,k}\sqrt{s/D_{s,k}} \cosh(r\sqrt{s/D_{s,k}})} \tag{4}$$

The pore wall flow rate,  $J_k$ , is usually calculated as:

$$J_k = \frac{R_{s,k}}{3A\varepsilon_{s,k}L_kF} I_L \tag{5}$$

where  $A$  is the electrode surface area,  $\varepsilon_s$  is the solid-phase volume fraction,  $F$  is the Faraday's constant,  $I_L$  is the load current.

Substituting Equation (5) into Equation (4), the standard transfer function expression of  $C_{s,k}$  can be rewritten as:

$$\frac{C_{s,k}(s)}{I_L(s)} = \frac{3A\varepsilon_{s,k}L_kFR_{s,k}}{D_{s,k}r} \frac{\sinh(r\sqrt{s/D_{s,k}})}{\sinh(r\sqrt{s/D_{s,k}}) - R_{s,k}\sqrt{s/D_{s,k}} \cosh(r\sqrt{s/D_{s,k}})} \tag{6}$$

In this study, Padé approximation is adopted to abate the solid-phase and liquid-phase diffusion processes of P2D model, which considers Padé approximation is more precise than the truncated Taylor series and typically still feasible when the Taylor series does not converge [20]. Since the active particle surface concentration,  $C_{surf}$  (at  $r = R_s$  position), is used to simulate the battery voltage behavior, the simplified expressions of  $C_{surf}$  with distinct orders according to Padé approximation are summarized in Table 1. More details involving Padé approximation re described in Ref. [20].

**Table 1.** The results of Padé approximation including different orders for  $C_{surf}$ .

Order	Active Particle Surface Concentration Expressions $C_{surf,k}(s)/I_L(s)$
1	$\pm \frac{1}{3AL_k\varepsilon_kF} \frac{3}{R_{s,k}} s$
2	$\pm \frac{1}{3AL_k\varepsilon_kF} \frac{3 + \frac{2R_{s,k}^2}{7D_{s,k}} s}{\frac{R_{s,k}^2}{s + \frac{D_{s,k}}{R_{s,k}}} s^2}$
3	$\pm \frac{1}{3AL_k\varepsilon_kF} \frac{3 + \frac{4R_{s,k}^2}{11D_{s,k}} s + \frac{R_{s,k}^4}{165D_{s,k}^2} s^2}{\frac{3R_{s,k}^2}{s + \frac{55D_{s,k}}{R_{s,k}}} s^2 + \frac{R_{s,k}^4}{3465D_{s,k}^2} s^3}$
4	$\pm \frac{1}{3AL_k\varepsilon_kF} \frac{3 + \frac{2R_{s,k}^2}{5D_{s,k}} s + \frac{2R_{s,k}^4}{195D_{s,k}^2} s^2 + \frac{4R_{s,k}^6}{75075D_{s,k}^3} s^3}{\frac{R_{s,k}^2}{s + \frac{15D_{s,k}}{R_{s,k}}} s^2 + \frac{2R_{s,k}^4}{2275D_{s,k}^2} s^3 + \frac{R_{s,k}^6}{675675D_{s,k}^3} s^4}$

### 2.2. Approximation of Liquid-Phase Diffusion Process of P2D

The liquid-phase diffusion process of P2D can be represented by Equation (7), which describes the diffusion process of lithium-ion between the positive and negative electrodes inside the battery. In Equation (6), the left side stands for the variation of dynamic concentration of electrolyte over time, and the right side represents the diffusion of lithium-ion in electrolyte based on Fick's second law, and the electro-migration process with electrolyte transport number,  $t_+^0$ , and the flow rate of the pore wall,  $J_k$ . Furthermore, the electrolyte

continuity inside the battery is described based on the boundary conditions given by Equation (8):

$$\epsilon_e \frac{\partial C_{e,dyn}(x,t)}{\partial t} = \frac{\partial}{\partial x} \left( D_e \frac{\partial C_{e,dyn}(x,t)}{\partial x} \right) + \frac{1-t_+^0}{F} J_k(t) \tag{7}$$

$$\begin{cases} \frac{\partial C_{e,dyn}}{\partial x} \Big|_{x=0} = \frac{\partial C_{e,dyn}}{\partial x} \Big|_{x=L_c} = 0 \\ D_e \frac{\partial C_{e,dyn}}{\partial x} \Big|_{x=L_n^-} = D_e \frac{\partial C_{e,dyn}}{\partial x} \Big|_{x=L_n^+}, C_{e,dyn} \Big|_{x=L_n^-} = C_{e,dyn} \Big|_{x=L_n^+} \\ D_e \frac{\partial C_{e,dyn}}{\partial x} \Big|_{x=L_p^-} = D_e \frac{\partial C_{e,dyn}}{\partial x} \Big|_{x=L_p^+}, C_{e,dyn} \Big|_{x=L_p^-} = C_{e,dyn} \Big|_{x=L_p^+} \end{cases} \tag{8}$$

where  $C_{e,dyn}$  is the dynamic concentration of electrolyte that varies with electrode thickness, current density, and the charging or discharging time,  $x = 0$  represents the negative current collector,  $x = L_c$  represents the positive current collector,  $L_c$  is the total thickness of the battery,  $x$  indicates the direction along the electrode thickness,  $D_e$  is the diffusion coefficient of electrolyte,  $\epsilon_e$  is the liquid-phase volume fraction.

Taking the Laplace transform to the variable  $t$  of Equation (7), the general solution for  $C_{e,dyn}$  in Equation (7) is solved as:

$$C_{e,dyn}(x,s) = D'_1 \exp\left(x\sqrt{\frac{\epsilon_e}{D_e}}s\right) + D'_2 \exp\left(x\sqrt{\frac{\epsilon_e}{D_e}}s\right) + \frac{BJ_k(s)}{s} \tag{9}$$

where  $D'_1$  and  $D'_2$  are the coefficients that should be determined, and  $B$  is calculated as:

$$B = \frac{1-t_0^+}{F\epsilon_e} \tag{10}$$

Substituting boundary conditions Equation (8) into Equation (9), the standard transfer function expression of  $C_{e,dyn}$  can be obtained as:

$$\frac{C_{e,dyn}(x,s)}{J_k(s)} = \frac{1-t_+^0}{F\epsilon_e} \frac{1}{s} \tag{11}$$

It can be seen that the transfer function expression (10) of dynamic electrolyte concentration obtained based on boundary conditions Equation (8) does not contain the parameter  $x$ , which means Equation (11) cannot depict the dynamic concentration behavior of electrolyte along the direction of electrode thickness during battery charging and discharging.

To deal with the problem, our previous study proposed the novel boundary conditions shown in Equation (12), where  $x = L_n + L_s$  stands for the positive electrode/separator boundary and  $x = L_n$  indicates the negative electrode/separator boundary.

$$\frac{\partial C_{e,dyn}}{\partial x} \Big|_{x=L_n} = -\frac{C_{e,dyn}(L_n)}{\frac{L_s+L_p-L_n}{2}}; \frac{\partial C_{e,dyn}}{\partial x} \Big|_{x=L_n+L_s} = \frac{C_{e,dyn}(L_n+L_s)}{\frac{L_s-L_p+L_n}{2}} \tag{12}$$

According to the proposed electrode/separator boundary conditions, the standard transfer function expression of dynamic concentration of electrolyte at the positive electrode current collector,  $C_{e,dyn}^p$ , can be obtained as in Equation (13), and the standard transfer function expression of electrolyte concentration at the negative electrode current collector,  $C_{e,dyn}^n$ , can be obtained as in Equation (14).

$$\frac{C_{e,dyn}^n(x,s) \Big|_{x=0}}{I_L(s)} = \frac{1-t_0^+}{AL_nF} \frac{2\sqrt{D_e} \left[ 1 - \cosh(L_n\sqrt{\frac{\epsilon_e}{D_e}}s) \right] + (-L_s - L_p + L_n)s^{\frac{1}{2}}\epsilon_e^{\frac{1}{2}} \sinh(L_n\sqrt{\frac{\epsilon_e}{D_e}}s)}{s^{\frac{3}{2}}\epsilon_e^{\frac{3}{2}}(-L_s - L_p + L_n) \sinh(L_n\sqrt{\frac{\epsilon_e}{D_e}}s) - 2\sqrt{D_e}\epsilon_e s \cosh(L_n\sqrt{\frac{\epsilon_e}{D_e}}s)} \tag{13}$$

$$\frac{C_{e,dyn}^P(x,s)|_{x=L_c}}{I_L(s)} = \frac{1 - t_0^+}{AL_p F} \frac{2\sqrt{D_e} \left[ \cosh(L_p \sqrt{\frac{\epsilon_e}{D_e} s}) - 1 \right] + (L_s + L_n - L_p) \epsilon_e \frac{1}{2} s^{\frac{1}{2}} \sinh(L_p \sqrt{\frac{\epsilon_e}{D_e} s})}{(L_s + L_n - L_p) \epsilon_e \frac{3}{2} s^{\frac{3}{2}} \sinh(L_p \sqrt{\frac{\epsilon_e}{D_e} s}) + 2\sqrt{D_e} \epsilon_e s \cosh(L_p \sqrt{\frac{\epsilon_e}{D_e} s})} \quad (14)$$

Applying the Padé approximation to Equations (13) and (14), the reduced expressions of dynamic electrolyte concentration with various orders according to Padé approximation are listed in Table 2.

**Table 2.** Padé approximation results of dynamic electrolyte concentrations with different orders.

Order	Dynamic Electrolyte Concentration Expressions $C_{e,dyn}(x,s)/I_L(s)$
1 ( $x = 0$ )	$-(1 - t_0^+) / (FA) \times 6(M - L_n)^2 / ((L_n \epsilon_e (-6M^2 + 10ML_n - 5L_n^2)s + 12D_e(M - L_n)))$ $(1 - t_0^+) / (FAL_n) \times (a_{1,n} + a_{2,n}(\epsilon_e / D_e)s) / (1 + b_{1,n}s + b_{2,n}(\epsilon_e / D_e)^2 s^2)$
2 ( $x = 0$ )	$a_{1,n} = (L_n^2 - ML_n) / (2D_e)$ $a_{2,n} = (-124M^3 L_n^3 + 139M^2 L_n^4 - 60ML_n^5 + 10L_n^6) / (168D_e(14M^2 - 12ML_n + 3L_n^2))$ $b_{1,n} = -(588M^3 L_n - 1020M^2 L_n^2 + 575ML_n^3 - 115L_n^4) / (84(14M^2 - 12ML_n + 3L_n^2))$ $b_{2,n} = -(-3720M^3 L_n^3 - 4302M^2 L_n^4 + 1878D_e ML_n^5 - 313L_n^6) / (70560M^2 - 60480ML_n + 15120L_n^2)$
1 ( $x = L_c$ )	$(1 - t_0^+) / (FA) \times 6(M^* + L_p)^2 / (L_p \epsilon_e (6M^{*2} + 10M^* L_p + 5L_p^2)s + 12D_e(M^* + L_p))$ $(1 - t_0^+) / (FAL_p) \times (a_{1,p} + a_{2,p}(\epsilon_e / D_e)s) / (1 + b_{1,p}s + b_{2,p}(\epsilon_e / D_e)^2 s^2)$
2 ( $x = L_c$ )	$a_{1,p} = (L_p^2 + ML_p) / (2D_e)$ $a_{2,p} = (124M^{*3} L_p^3 + 139M^{*2} L_p^4 + 60M^* L_p^5 + 10L_p^6) / (168D_e(14M^{*2} + 12M^* L_p + 3L_p))$ $b_{1,p} = (585M^{*3} L_p + 1020M^{*2} L_p^2 + 575M^* L_p^3 + 115L_p^4) / (84(14M^{*2} + 12M^* L_p + 3L_p^2))$ $b_{2,p} = (3720M^{*3} L_p^3 + 4320M^{*2} L_p^4 + 1878M^* L_p^5 + 313L_p^6) / (70560M^{*2} + 60480M^* L_p + 15120L_p^2)$

Where  $M = -L_s + L_p + L_n$ ;  $M^* = L_s + L_n - L_p$ .

### 2.3. Reduced P2D Model with Lumped Micro-Health Parameters

Based on the above reduced results of liquid-phase and solid-phase diffusion processes of the P2D model, 3-order reduced expression for  $C_{surf}$  and 2-order reduced expression for  $C_{e,dyn}$  are employed to simplify the terminal voltage of battery considering the model complexity and accuracy.

In the P2D model, the terminal voltage expression can be depicted as:

$$U_t = \underbrace{U_{ocv,p}(SOC_p - SOC_{p,0}) - U_{ocv,n}(SOC_n + SOC_{n,0})}_{\text{solid-phase diffusion related}} + \underbrace{\phi_{e,p} - \phi_{e,n}}_{\text{liquid-phase diffusion related}} + \underbrace{\eta_{act,p} - \eta_{act,n}}_{\text{electrochemical reaction related}} - \underbrace{R_{SEI} I_L}_{\text{SEI related}} \quad (15)$$

where  $U_{ocv,p}$  and  $U_{ocv,n}$  are the open circuit potential of the positive electrode and negative electrode, respectively;  $SOC_{p,0}$  and  $SOC_{n,0}$  are the initial lithium insertion of the negative electrode and positive electrode;  $SOC_n$  and  $SOC_p$  are the lithium insertion of the positive electrode and negative electrode, respectively;  $\phi_{e,p}$  and  $\phi_{e,n}$  are the liquid-phase potential of the positive electrode and negative electrode, respectively;  $\eta_{act,p}$  and  $\eta_{act,n}$  are the electrochemical reaction potential of the positive electrode and negative electrode, respectively;  $R_{SEI}$  is the solid/electrolyte interface impedance of active particle surface.

The expressions related to solid-phase diffusion can be further described as Equation (16); the expressions of  $U_{ocv,p}$  and  $U_{ocv,n}$  in Equation (14) can refer to Ref. [33].

$$\begin{cases} SOC_p = \frac{C_{surf,p}}{C_{max,p}} \\ SOC_n = \frac{C_{surf,n}}{C_{max,n}} \end{cases} \quad (16)$$

where,  $C_{max,n}$  is the maximum lithium insertion concentration of negative electrode.

### 2.3.1. Lumped Micro-Health Parameters Characterizing Electrolyte Performance

The liquid-phase potential difference between positive and negative electrodes can be calculated as follows:

$$(\phi_{e,p} - \phi_{e,n}) = \underbrace{(1 - t_0^+) \frac{2RT}{F} \ln \frac{C_{e,dyn}(s)|_{x=L_c}}{C_{e,dyn}(s)|_{x=0}}}_{\text{liquid-phase concentration overpotential}} - \underbrace{\frac{I_L}{2A} \left( \frac{L_n}{\kappa_e} + \frac{L_s}{\kappa_e} + \frac{L_p}{\kappa_e} \right)}_{\text{liquid-phase ohm overpotential}} \quad (17)$$

where,  $\kappa_e$  liquid-phase conductivity,  $T$  is the test environment temperature, and  $R$  is gas constant.

In the P2D model, the standard liquid-phase concentration overpotential is described as  $\eta_{con}$ , is written as:

$$\begin{aligned} \eta_{con}(s) &= \frac{2RT}{F} (1 - t_+^0) \ln \left( \frac{C_{e,dyn}(s)|_{x=L_c}}{C_{e,dyn}(s)|_{x=0}} \right) \\ &\approx \frac{2RT}{F} (1 - t_+^0) \left( \frac{C_{e,diff}(s)}{C_e} \right) \\ &= \frac{2RT}{F} (1 - t_+^0) \left( \frac{C_{e,dyn}(s)|_{x=L_c} - C_{e,dyn}(s)|_{x=0}}{C_e} \right) \end{aligned} \quad (18)$$

where,  $C_e$  is electrolyte concentration, which is the target parameter to be identified.

Substituting 2-order reduced expression for  $C_{e,dyn}$  into liquid-phase concentration overpotential section in Equation (18), the transfer function of liquid-phase concentration overpotential can be obtained as:

$$\frac{\eta_{con}(s)}{I_L(s)} = \frac{2RT}{C_e A} \left( \frac{1 - t_+^0}{F} \right)^2 \left( \frac{\frac{3(M^* + L_p)^2}{L_p \varepsilon_e (6M^{*2} + 10M^* L_p + 5L_p^2)s + 12D_e(M^* + L_p)} + }{L_n \varepsilon_e (-6M^2 + 10ML_n - 5L_n^2)s + 12D_e(M - L_n)} \right) \quad (19)$$

In this study, the target parameters characterizing electrolyte performance include electrolyte concentration,  $C_e$ , and diffusion coefficient,  $D_e$ . In the transfer functions of Equation (18),  $C_e$  and  $D_e$  are linked to other parameters. Hence, the two object parameters is not possible to be identified unambiguously. To tackle this issue, Equation (19) is rewritten as Equation (20).

$$\frac{\eta_{con}(s)}{I_L(s)} = \frac{\frac{0.58L_c}{D_e} \frac{2RT}{C_e A} \left( \frac{1 - t_+^0}{F} \right)^2}{\frac{0.58L_c}{D_e} \frac{2RT}{C_e A} \left( \frac{1 - t_+^0}{F} \right)^2 \times \frac{0.171C_e L_c A \varepsilon_e}{2RT \left( \frac{1 - t_+^0}{F} \right)^2} s + 1} \quad (20)$$

The parameters (except  $D_e$  and  $C_e$ ) are not influenced by the decomposition of the electrolyte. Therefore, the rest parameters are constant. Ultimately, Equation (20) can be rewritten as Equation (19), which is a reduced overpotential model of electrolyte concentration with lumped micro-health parameters,  $P_{D_e}$  and  $P_{C_e}$ .

$$\frac{\eta_{con}(s)}{I_L(s)} = \frac{P_{D_e}}{P_{D_e} P_{C_e} + 1} \quad (21)$$

where,

$$P_{D_e} = \frac{0.58L_c}{D_e} \frac{2RT}{C_e A} \left( \frac{1 - t_+^0}{F} \right)^2; P_{C_e} = \frac{0.171C_e L_c A \varepsilon_e}{2RT \left( \frac{1 - t_+^0}{F} \right)^2} \quad (22)$$

Since the changes in  $P_{D_e}$  and  $P_{C_e}$  are only determined by  $D_e$  and  $C_e$ ,  $P_{D_e}$  and  $P_{C_e}$  retain the physical significance of  $D_e$  and  $C_e$ . Consequently, the interference of non-target parameters on  $D_e$  and  $C_e$  can be dispelled.

### 2.3.2. Lumped Micro-Health Parameters Characterizing Electrolyte Performance

In P2D model, the micro-health parameters that can characterize negative electrode active material performance include negative electrode volume fraction,  $\varepsilon_n$ , and diffusion coefficient,  $D_{s,n}$ .

Since the change in the volume fraction of the active particles is directly related to the capacity loss of the electrode material, thus, the identification for  $\varepsilon_n$  can be converted to the identification of negative electrode capacity,  $Q_n$ . According to the electrode capacity definition, the mathematical relationship between  $Q_n$  and  $\varepsilon_n$  is described as Equation (23).

$$Q_n = AL_n C_{\max,n} \varepsilon_n F \quad (23)$$

Thus, the transfer function of solid-phase surface concentration is rewritten as:

$$\frac{C_{\text{surf},n}}{I_L} = \frac{C_{\max,n}}{3Q_n} \frac{3 + \frac{4R_n^2}{11D_{s,n}}s + \frac{R_n^4}{165D_{s,n}^2}s^2}{s + \frac{3R_n^2}{55D_{s,n}}s^2 + \frac{R_n^4}{3465D_{s,n}^2}s^3} \quad (24)$$

Based on Equation (16), Equation (24) can be rewritten as:

$$\frac{SOC_n}{I_L} = \frac{1200}{Q_n} \frac{3 + \frac{4R_n^2}{11D_{s,n}}s + \frac{R_n^4}{165D_{s,n}^2}s^2}{s + \frac{3R_n^2}{55D_{s,n}}s^2 + \frac{R_n^4}{3465D_{s,n}^2}s^3} \quad (25)$$

where the unit of  $Q_n$  is A·s in Equation (24), and the unit of  $Q_n$  is A·h in Equation (25).

Based on the above analysis, the identification for  $\varepsilon_n$  can be converted to the identification for  $Q_n$ , which eliminates the coupling effect of parameters such as electrode plate area on the volume fraction of active particles.

For diffusion coefficient of the negative electrode,  $D_s$ , since the continuous thickening of the SEI film lead to the solid-phase diffusion of lithium-ion weakened, and the thickened SEI film increases the active particle radius. The identification for  $D_{s,n}$  can be converted to identification for  $P_{D_{s,n}}$ , and Equation (25) can be rewritten as Equation (26), where,  $P_{D_{s,n}} = \frac{R_n^2}{D_{s,n}}$ .

$$\frac{SOC_n}{I_L} = \frac{1200}{Q_n} \frac{3 + \frac{4}{11}P_{D_{s,n}}s + \frac{1}{165}P_{D_{s,n}}^2s^2}{s + \frac{3}{35}P_{D_{s,n}}s^2 + \frac{1}{3465}P_{D_{s,n}}^2s^3} \quad (26)$$

The changes in  $\varepsilon_n$  and  $D_{s,n}$  are only determined by  $Q_n$  and  $P_{D_{s,n}}$ . Thus,  $Q_n$  and  $P_{D_{s,n}}$  maintain the physical significance of  $\varepsilon_n$  and  $D_s$ . Consequently, the interference of non-target parameters on  $\varepsilon_n$  and  $D_{s,n}$  can be dispelled. In addition, according to the stable performance of positive electrode material of LiFePO<sub>4</sub>/graphite battery,  $Q_p$  and  $P_{D_{s,p}}$  can be set as the experience values.

### 2.3.3. Reduced P2D Model

Since this study considers the identification of micro-health parameters characterizing negative electrode material and electrolyte performance, the other physical and chemical processes in the P2D model will be uniformly approximated as the ohmic overpotential.

Linearizing the Butler-Volmer equation of the electrochemical reaction process [34]:

$$\eta_k = \frac{RT}{i_k F} J_k = \pm \frac{1}{A} \frac{R_{s,k} RT}{3\varepsilon_k L_k i_k F^2}; \quad k = n, p \quad (27)$$

Thus, the electrochemical reaction overpotential,  $\eta_{\text{dif}}$ , is described as:

$$\begin{aligned}\eta_{\text{dif}} = \eta_{\text{p}} - \eta_{\text{n}} &= -\frac{I_{\text{L}}}{A} \left( \frac{R_{\text{p}}RT}{3\varepsilon_{\text{p}}L_{\text{p}}i_{\text{p}}F^2} + \frac{R_{\text{n}}RT}{3\varepsilon_{\text{n}}L_{\text{n}}i_{\text{n}}F^2} \right) \\ &= -\frac{1}{A} \left( \frac{R_{\text{p}}RT}{3\varepsilon_{\text{p}}L_{\text{p}}i_{\text{p}}F^2} + \frac{R_{\text{n}}RT}{3\varepsilon_{\text{n}}L_{\text{n}}i_{\text{n}}F^2} \right) \times I_{\text{L}}\end{aligned}\quad (28)$$

The liquid-phase ohmic overpotential of Equation (17) is described as:

$$\eta_{\text{e,ohm}} = -\frac{I_{\text{L}}}{2A} \left( \frac{L_{\text{n}}}{\kappa_{\text{e}}} + \frac{L_{\text{s}}}{\kappa_{\text{e}}} + \frac{L_{\text{p}}}{\kappa_{\text{e}}} \right) = -\frac{1}{2A} \left( \frac{L_{\text{n}}}{\kappa_{\text{e}}} + \frac{L_{\text{s}}}{\kappa_{\text{e}}} + \frac{L_{\text{p}}}{\kappa_{\text{e}}} \right) \times I_{\text{L}}\quad (29)$$

It can be seen that the model forms of Equations (28) and (29) can be written as the product of the invariant and the load current, and the lumped ohmic overpotential can be described as:

$$\begin{aligned}\eta_{\text{ohm}} &= -\frac{1}{2A} \left( \frac{L_{\text{n}}}{\kappa_{\text{e}}} + \frac{L_{\text{s}}}{\kappa_{\text{e}}} + \frac{L_{\text{p}}}{\kappa_{\text{e}}} \right) \times I_{\text{L}} - \frac{1}{A} \left( \frac{R_{\text{p}}RT}{3\varepsilon_{\text{p}}L_{\text{p}}i_{\text{p}}F^2} + \frac{R_{\text{n}}RT}{3\varepsilon_{\text{n}}L_{\text{n}}i_{\text{n}}F^2} \right) \times I_{\text{L}} + \frac{R_{\text{SEI}}F}{a_{\text{s}}} \times I_{\text{L}} \\ &= P_{\text{ohm}} \times I_{\text{L}}\end{aligned}\quad (30)$$

where  $P_{\text{ohm}}$  is the lumped ohmic resistance to be identified.

Based on the above lumped-parameter method, the reduced P2D model is described as:

$$\begin{cases} U_{\text{t}} = U_{\text{ocv,p}}(\text{SOC}_{\text{p},0} - \text{SOC}_{\text{p}}) - U_{\text{ocv,n}}(\text{SOC}_{\text{n},0} + \text{SOC}_{\text{n}}) + \eta_{\text{con}} + P_{\text{ohm}} \times I_{\text{L}} \\ \frac{\text{SOC}_{\text{p}}}{I_{\text{L}}} = -\frac{1200}{Q_{\text{p}}} \frac{3 + \frac{4}{11}P_{\text{D}_{\text{s,p}}}s + \frac{1}{165}P_{\text{D}_{\text{s,p}}}^2s^2}{s + \frac{3}{35}P_{\text{D}_{\text{s,p}}}s^2 + \frac{1}{3465}P_{\text{D}_{\text{s,p}}}^2s^3} \\ \frac{\text{SOC}_{\text{n}}}{I_{\text{L}}} = \frac{1200}{Q_{\text{n}}} \frac{3 + \frac{4}{11}P_{\text{D}_{\text{s,n}}}s + \frac{1}{165}P_{\text{D}_{\text{s,n}}}^2s^2}{s + \frac{3}{35}P_{\text{D}_{\text{s,n}}}s^2 + \frac{1}{3465}P_{\text{D}_{\text{s,n}}}^2s^3} \\ \frac{\eta_{\text{con}}(s)}{I_{\text{L}}(s)} = \frac{P_{\text{D}_{\text{e}}}}{P_{\text{D}_{\text{e}}}P_{\text{C}_{\text{e}}}s + 1}\end{cases}\quad (31)$$

### 3. Fast Identification of the Target Micro-Health Parameters Based on the Reduced P2D Model

To fast identify the target micro-health parameters including  $Q_{\text{n}}$ ,  $P_{\text{D}_{\text{s,n}}}$ ,  $P_{\text{D}_{\text{e}}}$ , and  $P_{\text{C}_{\text{e}}}$ , which characterize negative electrode active material ( $Q_{\text{n}}$  and  $P_{\text{D}_{\text{s,n}}}$ ) and electrolyte ( $P_{\text{D}_{\text{e}}}$  and  $P_{\text{C}_{\text{e}}}$ ) performance, the constant-current charging condition which is the necessary test process for retired batteries, is employed in this study to shorten the test time of retired batteries. As the basis for accurate parameter identification, parameter sensitivity analysis under constant-current charging conditions is performed first in this section. Based on the parameter sensitivity analysis results, the fast identification strategy of the target micro-health parameters under constant-current charging conditions is proposed, subsequently.

#### 3.1. Sensitivity Analysis of Target Micro-Health Parameters

Sensitivity analysis refers to the degree of dispersion of battery terminal voltage resulted from model parameters fluctuating within a certain range. The higher dispersion indicates that the terminal voltage is highly sensitive to the model parameters. Since the sensitivity of battery voltage to parameters  $\varepsilon_{\text{n}}$ ,  $D_{\text{s,n}}$ ,  $C_{\text{e}}$  and  $D_{\text{e}}$  is consistent with  $Q_{\text{n}}$ ,  $P_{\text{D}_{\text{s,n}}}$ ,  $P_{\text{C}_{\text{e}}}$ , and  $P_{\text{D}_{\text{e}}}$ , herein,  $Q_{\text{n}}$ ,  $D_{\text{s,n}}$ ,  $C_{\text{e}}$ , and  $D_{\text{e}}$  are divided into ten equal intervals within a certain range. Each value of  $Q_{\text{n}}$ ,  $D_{\text{s,n}}$ ,  $C_{\text{e}}$ , and  $D_{\text{e}}$  within a certain range is simulated under constant-current charging conditions, and the effects on battery terminal voltage are analyzed and discussed. To observe the sensitivity of the battery terminal voltage to the parameter changes more clearly, the change ranges of target parameters are appropriately increased in this study. Table 3 shows the value change range of  $Q_{\text{n}}$ ,  $D_{\text{s,n}}$ ,  $C_{\text{e}}$ , and  $D_{\text{e}}$ , and the sensitivity simulation results under 0.5 C and 1 C constant-current charging condition are plotted from Figures 2–5.

**Table 3.** Parameter ranges setting.

Parameter	Value Ranges
$Q_n$ (Ah)	7~8
$D_{s,n}$ (m <sup>2</sup> /s)	$2.894 \times 10^{-14}$ ~ $2.412 \times 10^{-14}$
$D_e$ (m <sup>2</sup> /s)	$0.7 \times 10^{-11}$ ~ $1.88 \times 10^{-11}$
$C_e$ (mol/m <sup>3</sup> )	600~1500

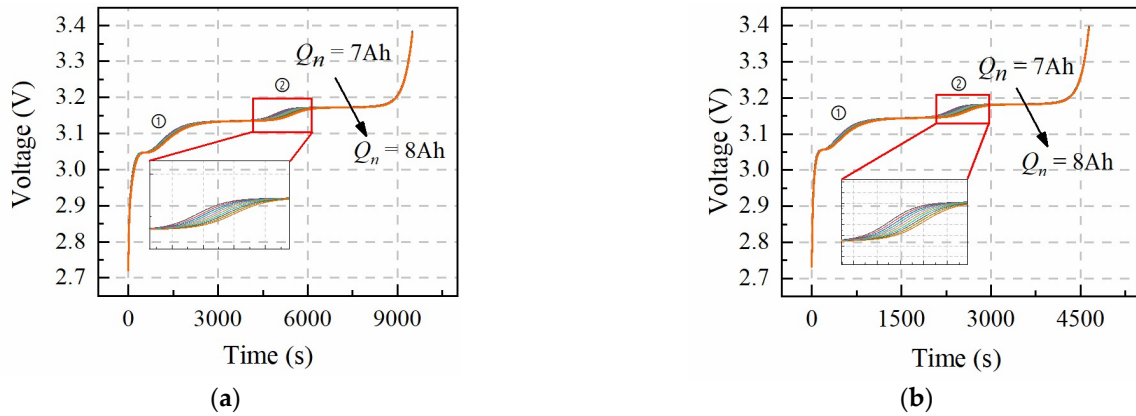


**Figure 2.** Sensitivity curves of battery terminal voltage to  $Q_n$  under different charging rates. (a) Sensitivity curves under 0.5 C charging; (b) Sensitivity curves under 1 C charging.

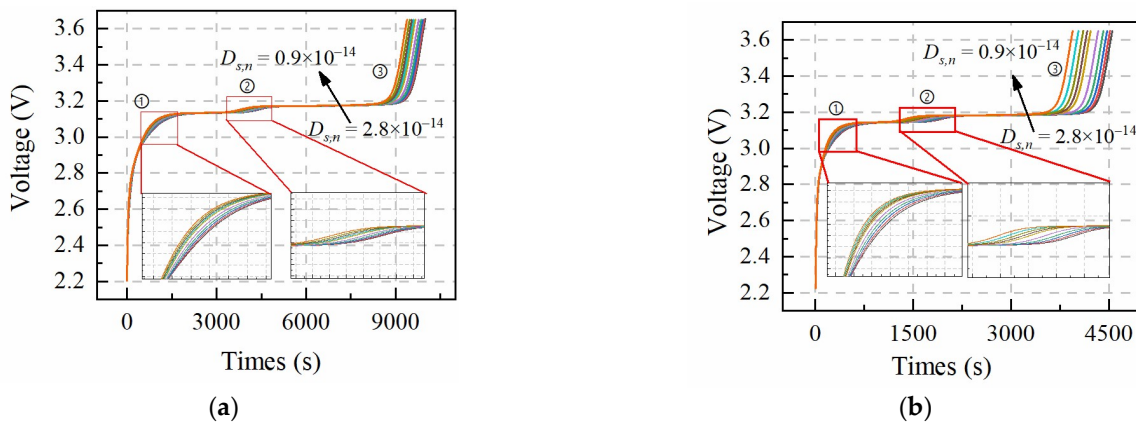


**Figure 3.** Sensitivity curves of battery terminal voltage to  $D_{s,n}$  under different charging rates. (a) Sensitivity curves under 0.5 C charging rate; (b) Sensitivity curves under 1 C charging rate.

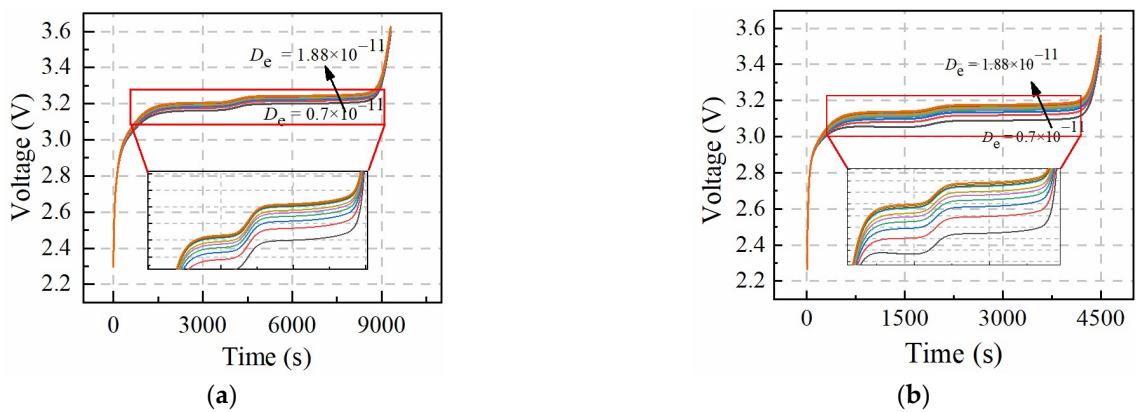


**Figure 4.** Sensitivity curves of battery terminal voltage to  $D_e$  under different charging rates. (a) Sensitivity curves under 0.5 C charging rate; (b) Sensitivity curves under 1 C charging rate.

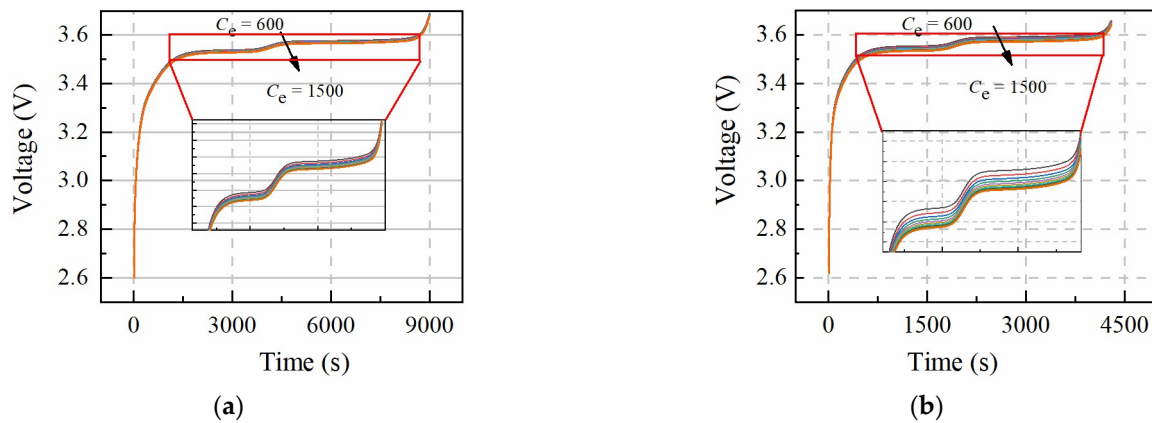


**Figure 5.** Sensitivity curves of battery terminal voltage to  $C_e$  under different charging rates. (a) Sensitivity curves under 0.5 C charging rate; (b) Sensitivity curves under 1 C charging rate.

Figure 2 shows that the influence of the changes in  $Q_n$  on the voltage curve is not consistent throughout the whole charging process with different charging rates. Number ① and ② positions of the voltage curve bundle present the discrete phenomenon, and the curve bundle at other positions during the charging process is almost overlapped. This phenomenon indicates that micro-health parameters,  $Q_n$ , can be identified at number ① and ② positions under the constant-current charging condition. In addition, the sensitivity of  $Q_n$  on the battery voltage bundle under 0.5 C and 1 C constant-current charging conditions exhibit the same results, which means the accurate identification of  $Q_n$  has nothing to do with the current rate and can be obtained under the larger rate constant-current charging condition.

In Figure 3, the sensitivity of  $D_{s,n}$  to the terminal voltage shows similar results to  $Q_n$  at number ① and ② positions. The difference from  $Q_n$  is at the number ③ position of the constant-current charging curve bundle. Since the decrease of  $D_{s,n}$  leads to the larger difference between the average and surface Li-ion concentration of active particles, the larger concentration difference will cause the battery to trigger the upper voltage limit in advance. In addition, the degree of dispersion of voltage curves at number ①, ② and ③ positions is obvious under the 1 C charging condition, which means  $D_{s,n}$  is relatively easy to be identified under the larger charging rate.

Based on the sensitivity analysis results,  $Q_n$  and  $P_{D_{s,n}}$  can be identified at number ① and ② positions of the larger constant-charging condition. The difference of number ③ between  $Q_n$  and  $P_{D_{s,n}}$  makes that  $P_{D_{s,n}}$  can be identified more accurately.

Figures 4 and 5 show the sensitivity of  $D_e$  and  $C_e$  to constant-current charging voltage, which presents similar results. The larger current rate causes the voltage curve dispersion to increase, which means  $P_{D_e}$  and  $P_{C_e}$  are easily identified under the larger rate constant-current charging condition. The sensitivity of  $D_e$  and  $C_e$  to the voltage curves is different from  $Q_n$  and  $D_{s,n}$ , which means  $P_{C_e}$  and  $P_{D_e}$  can be identified at the same constant-current charging condition.

### 3.2. Fast Identification Method of Micro-Health Parameters

Based on the above sensitivity analysis results, the sensitivity degrees of  $Q_n$ ,  $D_{s,n}$ ,  $D_e$ , and  $C_e$  to battery terminal voltage are varying, especially under the large-range constant-current charging condition, which means the identification of  $Q_n$ ,  $P_{D_{s,n}}$ ,  $P_{D_e}$ , and  $P_{C_e}$  can be achieved under larger constant-current charging condition.

In this study,  $Q_n$  and  $P_{D_{s,n}}$  are identified first according to the different sensitivity results with  $P_{D_e}$  and  $P_{C_e}$ . To identify the micro-health parameters,  $Q_n$  and  $P_{D_{s,n}}$ , the electrolyte concentration overpotential part of the terminal voltage expression is temporarily integrated into the ohmic internal resistance section,  $P'_{Rohm}$ , and Equation (15) is rewritten as Equation (32).

$$U_t = U_{ocv,p}(SOC_{p,0} - \frac{\int I_L dt}{Q_p}) - U_{ocv,n}(SOC_{n,0} + \frac{\int I_L dt}{Q_n}) + P'_{Rohm} \times I_L \quad (32)$$

where,  $P'_{Rohm} = P_{Rohm} + \eta_{con}$ .

Based on the Equations (26) and (32), the micro-health parameters  $Q_n$  and  $P_{D_{s,n}}$  can be identified with the pattern search optimization algorithm, the detailed calculation procedures which are reported in our previous paper [35].

To eliminate the impact of ohmic internal resistance on the identification results of micro-health parameters related to electrolyte performance, the ohmic internal resistance should be obtained at the moment of charging shown in Equation (33), which considers the response time of ohmic overpotential is shorter than concentration polarization overpotential.

$$P_{Rohm} = \frac{U_2 - U_1}{I_L} \quad (33)$$

where,  $U_1$  is the moment before charging;  $U_2$  is the start of charging.

After the micro-health parameters  $Q_n$  and  $P_{D_{s,n}}$ , are confirmed, subsequently,  $P_{D_e}$  and  $P_{C_e}$  are extracted under constant-current charging condition with the pattern search optimization algorithm.

The flowchart of the proposed fast identification method for micro-health parameters ( $Q_n, P_{D_s}, P_{D_e}, P_{C_e}$ ) is shown in Figure 6.

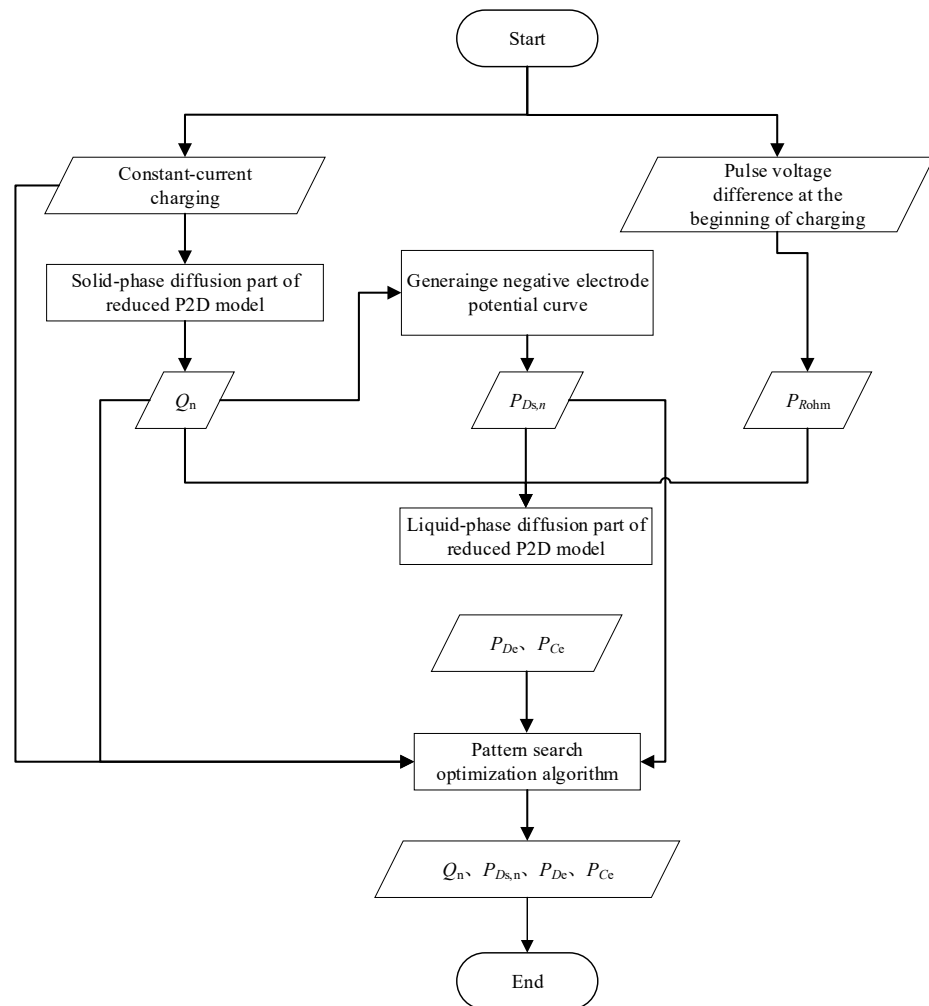
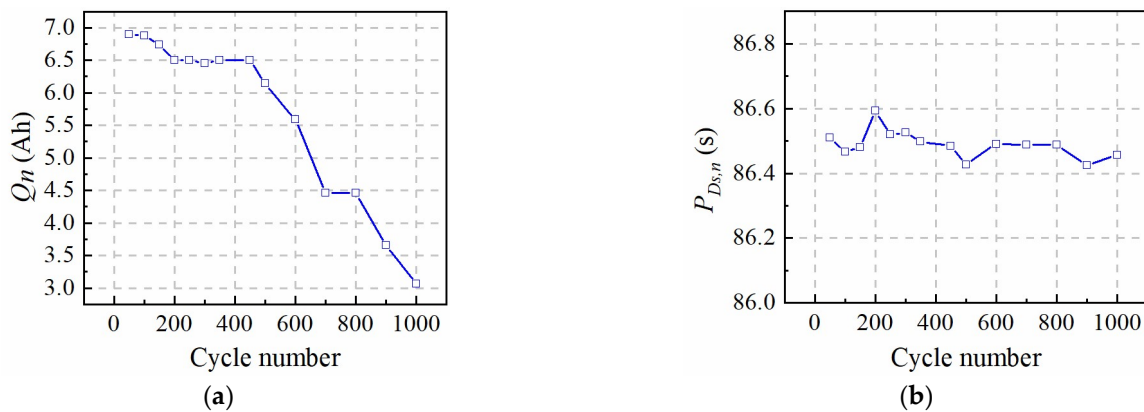


Figure 6. The flowchart of fast identification procedures for micro-health parameters ( $Q_n, P_{D_s}, P_{D_e}, P_{C_e}$ ).

## 4. Results and Discussion

### 4.1. Identification Results of Micro-Health Parameters

In order to verify the accuracy of the proposed micro-health parameter identification method, the aging tests of 32,650 cylindrical LiFePO<sub>4</sub>/C are carried out under the condition of the 1 C charge-discharge cycle. Based on the identification strategy proposed in Section 3, the identification result of micro-health parameters including  $Q_n$ ,  $P_{D_{s,n}}$ ,  $P_{D_e}$ , and  $P_{C_e}$  under 1 C constant-current charging condition is plotted in Figures 7 and 8. As the aging degree of the battery intensifies, the negative electrode material of the tested battery is lost, but the diffusion capacity of lithium ions inside the negative electrode active particle has not changed significantly. For the electrolyte, it was apparent that as the battery aging degree intensifies, the lithium-ion diffusion capacity in electrolyte shows a weakening trend, while the electrolyte concentration shows an increasing trend, which is caused by the side reactions inside the battery that consumes the solvent in the electrolyte during the aging process.



**Figure 7.** The identification results of health characteristic parameters of the negative electrode. (a) Negative electrode capacity; (b) Solid-phase diffusion ability.

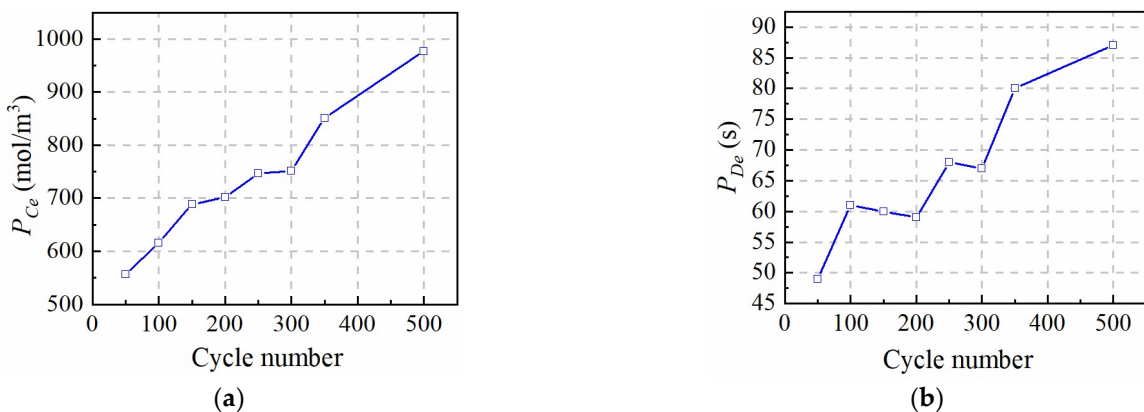


**Figure 8.** The identification results of health characteristic parameters of electrolyte. (a) Electrolyte concentration; (b) Liquid-phase diffusion ability.

### 4.2. Result Verification and Analysis

To verify the identification results accuracy of the micro-health parameters  $Q_n$  and  $P_{D_{s,n}}$ , Figure 9 compares the terminal voltage simulation outcomes obtained from the identified micro-health parameters under different aging states with the real measured voltage curve. It is found that the simulation outcomes can well fit the experimental voltage at number ① and ② positions that correspond to the higher sensitivity of battery voltage to parameters  $\varepsilon_n$  and  $D_{s,n}$ . The micro-health parameters  $Q_n$  and  $P_{D_{s,n}}$  can be identified by the

charging voltage domain that contains the obvious phase transition of the battery negative electrode.

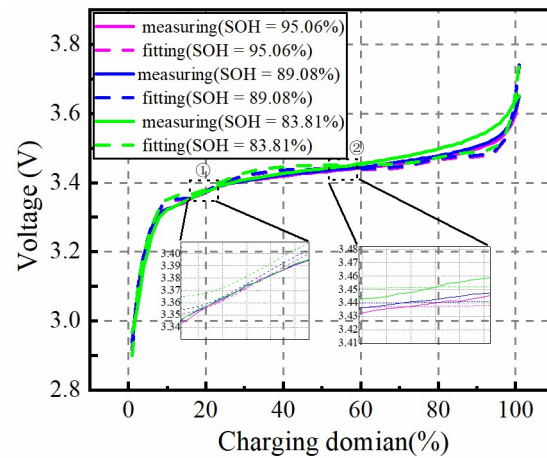


Figure 9. Validation of identification results of  $Q_n$  and  $P_{D_{s,n}}$ .

To verify the identification results of the micro-health parameters  $P_{D_e}$  and  $P_{C_e}$ , Figure 10 shows that the simulation curve on the basis of the identified parameters can fit well with the measurement curve, which means  $P_{D_e}$  and  $P_{C_e}$  are accurately identified. Table 4 compares the identification time in our study and other research in Refs. [30,31]. Although the number of identified parameters is reduced, our study shortens the identification time of the characteristic parameters that characterize the health of the battery’s negative electrode material and electrolyte, and avoids the design of complex parameter identification conditions.

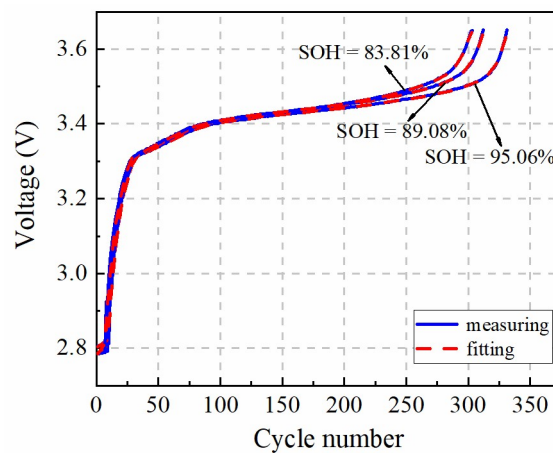


Figure 10. The validation of identification results of  $P_{D_e}$  and  $P_{C_e}$ .

Table 4. Comparison of test time under different identification conditions.

Identified Parameters	Intensification Condition	Test Time
28 micro-health parameters including volume fraction of positive and negative active particles, etc. [30]	Multi-rate composite pulse test	63 min
17 micro-health parameters including positive/negative electrode capacity, solid/liquid phase diffusion coefficient, etc. [31]	① Small rate constant-current test	25 h
	② Multi-rate composite pulse test	
	③ Electrochemical impedance spectroscopy test	
4 micro-health parameters related to negative electrode material and electrolyte	1 C constant-current charging test (this work)	45 min

## 5. Conclusions

In this paper, a fast identification approach for micro-health parameters characterizing negative electrode material and electrolyte performance of  $\text{LiFePO}_4$  is proposed according to the reduced P2D model with Páde approximation. As the basis of micro-health parameter identification, diffusion processes of the liquid-phase and solid-phase of the P2D model are simplified with the Páde approximation method, respectively. Considering the analytical solution for the liquid-phase diffusion process cannot depict the dynamic performance of electrolyte concentration during charge or discharge condition, the improved boundary conditions for the P2D model are proposed to solve this problem. Based on the simplified solid-phase and liquid-phase diffusion expressions, a new battery terminal voltage model with lumped parameters for  $\varepsilon_n$ ,  $D_{s,n}$ ,  $D_e$  and  $C_e$  are developed. In this model, these target parameters and the other parameters of the P2D model, are lumped together, eliminating the coupling effects of non-target parameters on the coverage results of  $\varepsilon_n$ ,  $D_{s,n}$ ,  $D_e$ , and  $C_e$ . These lumped parameters are recognized based on the nonlinear optimization of pattern search, and the identification accuracy of the lumped parameters is verified under 1 C constant-current charging condition, which improves the parameter identification efficiency compared with other two identification methods. According to the above definite findings, the fast identification method for micro-health parameters characterizing negative electrode material and electrolyte performance can provide a multi-dimensional sorting basis for the second-use application of retired batteries from electric vehicles, and improve the performance consistency of regrouped retired batteries.

To be clear, for the high-rate charge or discharge condition, the uniform distribution of particle sizes need to be considered based on the proposed model in this study.

**Author Contributions:** J.X.: Methodology, Software, Writing—Original draft preparation, Validation. C.S.: Software, Writing—Reviewing and Editing. Y.N.: Writing—Reviewing and Editing, Investigation. C.L.: Conceptualization, Funding acquisition, Writing—Reviewing. C.W.: Writing—Reviewing and Editing, Data Curation. H.Z.: Writing—Reviewing and Editing, Conceptualization. Q.Y.: Writing—Reviewing and Editing, Formal analysis. F.F.: Supervision, Project administration. All authors have read and agreed to the published version of the manuscript.

**Funding:** This research was funded by the China Postdoctoral Science Foundation, grant number 2021M701017.

**Data Availability Statement:** The data presented in this study are available on request from the corresponding author. The data are not publicly available due to long-time experiment and rich information.

**Conflicts of Interest:** The authors declare no conflict of interest.

## Abbreviations

EVs	electric vehicles
P2D	pseudo-two-dimensional
SP	single-particle
ESP	extended single-particle

## Subscripts

surf	surface concentration
s	solid
max	maximum concentration
con	concentration
dif	difference value
dyn	dynamic electrolyte concentration
L	load current
e	electrolyte
k	n, sep or p (negative electrode/separator/positive electrode)
n	negative electrode

p	positive electrode
sep	separator
c	total electrode thickness
t	time step
con	concentration
ocv	open circuit potential
act	electrochemical reaction

## References

- Hu, X.; Xu, L.; Lin, X.; Pecht, M. Battery Lifetime Prognostics. *Joule* **2020**, *4*, 310–346. [[CrossRef](#)]
- Jiang, Z.Y.; Qu, Z.G.; Zhang, J.F.; Rao, Z.H. Rapid Prediction Method for Thermal Runaway Propagation in Battery Pack Based on Lumped Thermal Resistance Network and Electric Circuit Analogy. *Appl. Energy* **2020**, *268*, 115007. [[CrossRef](#)]
- Feng, F.; Yang, R.; Meng, J.; Xie, Y.; Zhang, Z.; Chai, Y.; Mou, L. Electrochemical Impedance Characteristics at Various Conditions for Commercial Solid–Liquid Electrolyte Lithium-Ion Batteries: Part 1. Experiment Investigation and Regression Analysis. *Energy* **2021**, *242*, 122880. [[CrossRef](#)]
- Müller, D.; Dufaux, T.; Birke, K.P. Model-Based Investigation of Porosity Profiles in Graphite Anodes Regarding Sudden-Death and Second-Life of Lithium Ion Cells. *Batteries* **2019**, *5*, 49. [[CrossRef](#)]
- Quinard, H.; Redondo-Iglesias, E.; Pelissier, S.; Venet, P. Fast Electrical Characterizations of High-Energy Second Life Lithium-Ion Batteries for Embedded and Stationary Applications. *Batteries* **2019**, *5*, 33. [[CrossRef](#)]
- Ni, Y.; Xu, J.; Zhu, C.; Pei, L. Accurate Residual Capacity Estimation of Retired LiFePO<sub>4</sub> Batteries Based on Mechanism and Data-Driven Model. *Appl. Energy* **2022**, *305*, 117922. [[CrossRef](#)]
- Lai, X.; Huang, Y.; Deng, C.; Gu, H.; Han, X.; Zheng, Y.; Ouyang, M. Sorting, Regrouping, and Echelon Utilization of the Large-Scale Retired Lithium Batteries: A Critical Review. *Renew. Sustain. Energy Rev.* **2021**, *146*, 111162. [[CrossRef](#)]
- Li, X.; Fan, G.; Rizzoni, G.; Canova, M.; Zhu, C.; Wei, G. A simplified multi-particle model for lithium ion batteries via a predictor-corrector strategy and quasi-linearization. *Energy* **2016**, *116*, 154–169. [[CrossRef](#)]
- Jokar, A.; Rajabloo, B.; Desilets, M.; Lacroix, M. Review of simplified Pseudo-Two-Dimensional models of lithium-ion batteries. *J. Power Sources* **2016**, *327*, 44–55. [[CrossRef](#)]
- Guo, M.; Sikha, G.; White, R.E. Single-Particle Model for a Lithium-Ion Cell: Thermal Behavior. *J. Electrochem. Soc.* **2011**, *158*, A122. [[CrossRef](#)]
- Zhang, Q.; White, R.E. Comparison of Approximate Solution Methods for the Solid Phase Diffusion Equation in a Porous Electrode Model. *J. Power Sources* **2007**, *165*, 880–886. [[CrossRef](#)]
- Baba, N.; Yoshida, H.; Nagaoka, M.; Okuda, C.; Kawauchi, S. Numerical Simulation of Thermal Behavior of Lithium-Ion Secondary Batteries Using the Enhanced Single Particle Model. *J. Power Sources* **2014**, *252*, 214–228. [[CrossRef](#)]
- Han, X.; Ouyang, M.; Lu, L.; Li, J. Simplification of Physics-Based Electrochemical Model for Lithium Ion Battery on Electric Vehicle. Part I: Diffusion Simplification and Single Particle Model. *J. Power Sources* **2015**, *278*, 802–813. [[CrossRef](#)]
- Han, X.; Ouyang, M.; Lu, L.; Li, J. Simplification of Physics-Based Electrochemical Model for Lithium Ion Battery on Electric Vehicle. Part II: Pseudo-Two-Dimensional Model Simplification and State of Charge Estimation. *J. Power Sources* **2015**, *278*, 814–825. [[CrossRef](#)]
- Luo, W.; Lyu, C.; Wang, L.; Zhang, L. A New Extension of Physics-Based Single Particle Model for Higher Charge-Discharge Rates. *J. Power Sources* **2013**, *241*, 295–310. [[CrossRef](#)]
- Grzywna, Z.J.; Petropoulos, J.H. New Separation of Variables Method for Composite Electrodes with Galvanostatic Boundary Conditions. *J. Chem. Soc. Faraday Trans. 2* **1983**, *79*, 571–584. [[CrossRef](#)]
- Subramanian, V.R.; Diwakar, V.D.; Tapriyal, D. Efficient Macro-Micro Scale Coupled Modeling of Batteries. *J. Electrochem. Soc.* **2005**, *152*, A2002–A2008. [[CrossRef](#)]
- Cai, L.; White, R.E. Reduction of Model Order Based on Proper Orthogonal Decomposition for Lithium-Ion Battery Simulations. *J. Electrochem. Soc.* **2009**, *156*, A154–A161. [[CrossRef](#)]
- Cai, L.; White, R.E. An Efficient Electrochemical–Thermal Model for a Lithium-Ion Cell by Using the Proper Orthogonal Decomposition Method. *J. Electrochem. Soc.* **2010**, *157*, A1188–A1195. [[CrossRef](#)]
- Marcicki, J.; Canova, M.; Conlisk, A.T.; Rizzoni, G. Design and Parametrization Analysis of a Reduced-Order Electrochemical Model of Graphite/LiFePO<sub>4</sub> Cells for SOC/SOH Estimation. *J. Power Sources* **2013**, *237*, 310–324. [[CrossRef](#)]
- Fan, G.; Pan, K.; Canova, M.; Marcicki, J.; Yang, X.G. Modeling of Li-Ion Cells for Fast Simulation of High C-Rate and Low Temperature Operations. *J. Electrochem. Soc.* **2016**, *163*, A666–A676. [[CrossRef](#)]
- Li, X.; Fan, G.; Pan, K.; Wei, G.; Zhu, C.; Rizzoni, G.; Canova, M. A Physics-Based Fractional Order Model and State of Energy Estimation for Lithium Ion Batteries. Part I: Model Development and Observability Analysis. *J. Power Sources* **2017**, *367*, 187–201. [[CrossRef](#)]
- Santhanagopalan, S.; Guo, Q.; White, R.E. Parameter Estimation and Model Discrimination for a Lithium-Ion Cell. *J. Electrochem. Soc.* **2007**, *154*, A198–A206. [[CrossRef](#)]
- Santhanagopalan, S.; Zhang, Q.; Kumaresan, K.; White, R.E. Parameter Estimation and Life Modeling of Lithium-Ion Cells. *J. Electrochem. Soc.* **2008**, *155*, A345–A353. [[CrossRef](#)]

25. Jokar, A.; Rajabloo, B.; Désilets, M.; Lacroix, M. An Inverse Method for Estimating the Electrochemical Parameters of Lithium-Ion Batteries. *J. Electrochem. Soc.* **2016**, *163*, A2876–A2886. [[CrossRef](#)]
26. Rajabloo, B.; Jokar, A.; Désilets, M.; Lacroix, M. An Inverse Method for Estimating the Electrochemical Parameters of Lithium-Ion Batteries. *J. Electrochem. Soc.* **2017**, *164*, A99–A105. [[CrossRef](#)]
27. Jokar, A.; Rajabloo, B.; Desilets, M.; Lacroix, M. An On-Line Electrochemical Parameter Estimation Study of Lithium-Ion Batteries Using Neural Networks. *ECS Trans.* **2017**, *75*, 73–87. [[CrossRef](#)]
28. Han, X.; Ouyang, M.; Lu, L.; Li, J.; Zheng, Y.; Li, Z. A Comparative Study of Commercial Lithium Ion Battery Cycle Life in Electrical Vehicle: Aging Mechanism Identification. *J. Power Sources* **2014**, *251*, 38–54. [[CrossRef](#)]
29. Masoudi, R.; Uchida, T.; McPhee, J. Parameter Estimation of an Electrochemistry-Based Lithium-Ion Battery Model. *J. Power Sources* **2015**, *291*, 215–224. [[CrossRef](#)]
30. Zhang, L.; Wang, L.; Hinds, G.; Lyu, C.; Zheng, J.; Li, J. Multi-Objective Optimization of Lithium-Ion Battery Model Using Genetic Algorithm Approach. *J. Power Sources* **2014**, *270*, 367–378. [[CrossRef](#)]
31. Li, J.; Wang, L.; Lyu, C.; Wang, H.; Liu, X. New Method for Parameter Estimation of an Electrochemical-Thermal Coupling Model for LiCoO<sub>2</sub> Battery. *J. Power Sources* **2016**, *307*, 220–230. [[CrossRef](#)]
32. Li, X.; Pan, K.; Fan, G.; Lu, R.; Zhu, C.; Rizzoni, G.; Canova, M. A Physics-Based Fractional Order Model and State of Energy Estimation for Lithium Ion Batteries. Part II: Parameter Identification and State of Energy Estimation for LiFePO<sub>4</sub> Battery. *J. Power Sources* **2017**, *367*, 202–213. [[CrossRef](#)]
33. Safari, M.; Delacourt, C. Modeling of a Commercial Graphite/LiFePO<sub>4</sub> Cell. *J. Electrochem. Soc.* **2011**, *158*, A562–A571. [[CrossRef](#)]
34. Smith, K.A.; Rahn, C.D.; Wang, C.Y. Control Oriented 1D Electrochemical Model of Lithium Ion Battery. *Energy Convers. Manag.* **2007**, *48*, 2565–2578. [[CrossRef](#)]
35. Xu, J.; Wang, T.; Pei, L.; Mao, S.; Zhu, C. Parameter Identification of Electrolyte Decomposition State in Lithium-Ion Batteries Based on a Reduced Pseudo Two-Dimensional Model with Padé Approximation. *J. Power Sources* **2020**, *460*, 228093. [[CrossRef](#)]

**Disclaimer/Publisher’s Note:** The statements, opinions and data contained in all publications are solely those of the individual author(s) and contributor(s) and not of MDPI and/or the editor(s). MDPI and/or the editor(s) disclaim responsibility for any injury to people or property resulting from any ideas, methods, instructions or products referred to in the content.